Electronic Supplementary Material (ESI) for Dalton Transactions.
This journal is © The Royal Society of Chemistry 2019

Electronic Supplementary Information

Rational design and green synthesis of 3D metal organic frameworks comprised of a rigid heterocyclic nitrogen-rich dicarboxylate: structural diversity, CO_2 sorption and selective sensing of 2,4,6-TNP in water†

Alisha Gogia and Sanjay K. Mandal*

Department of Chemical Sciences, Indian Institute of Science Education and Research Mohali, Sector 81, Manauli PO, S.A.S. Nagar, Mohali, Punjab 140306, INDIA

*Author for correspondence:
Prof. Sanjay K. Mandal, E-mail: sanjaymandal@iisermohali.ac.in.

Table of Contents

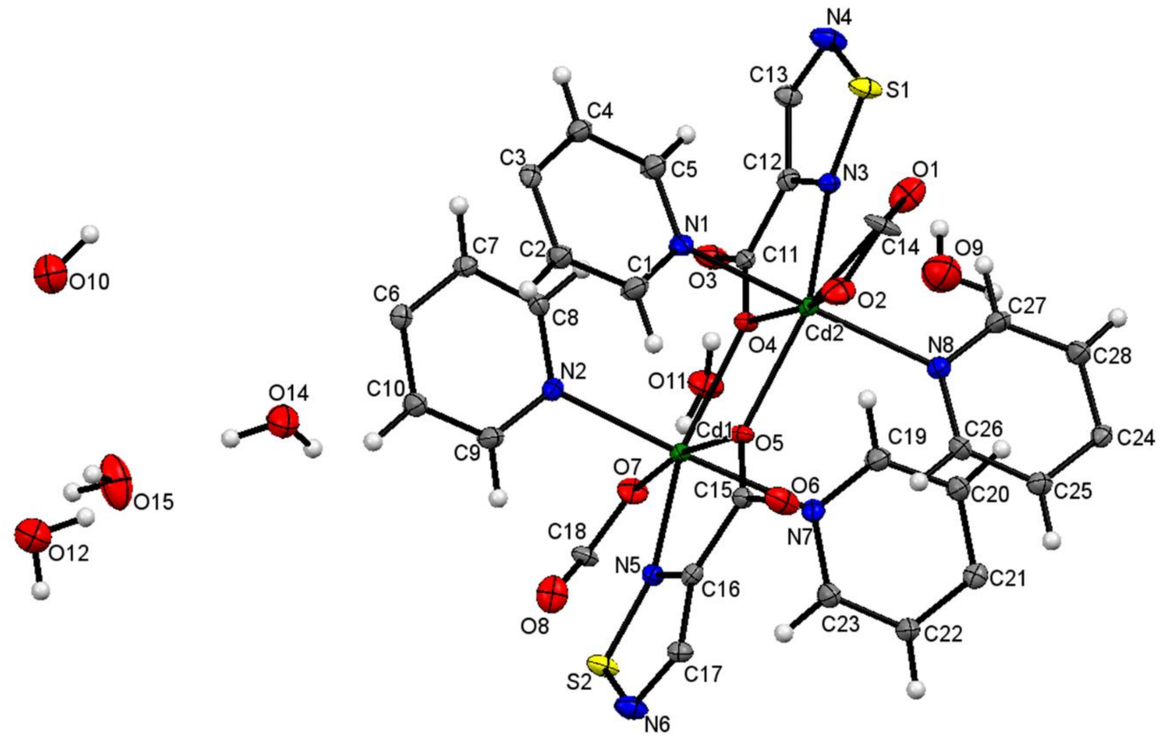

Fig. S1 ORTEP view of the asymmetric unit in **1**.

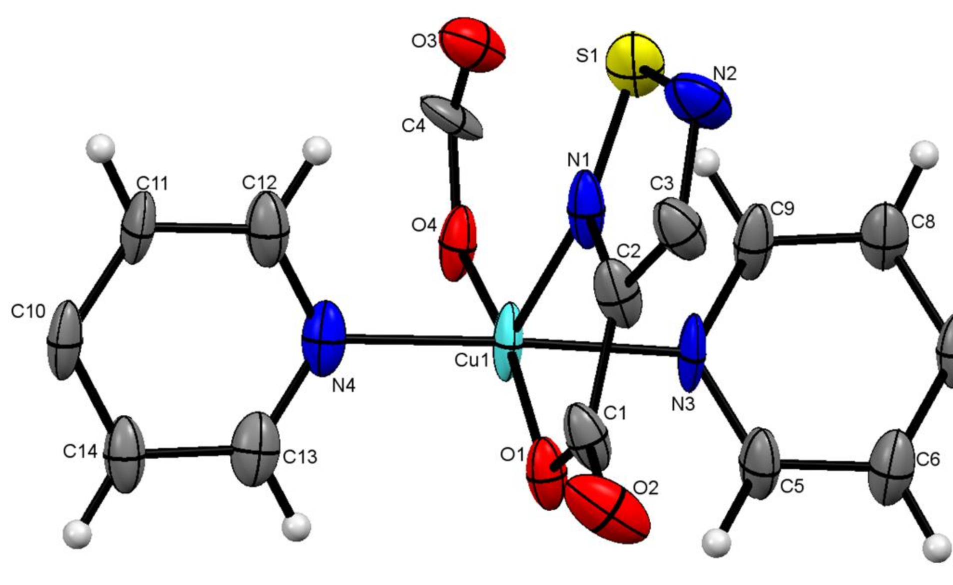

Fig. S2 ORTEP view of the asymmetric unit in **2**.

Table S1. Selected bond lengths (Å) and angles (°) for **1**.

Bond distances (Å)

Cd1-O7	2.2541(19)	Cd1-O4	2.2897(17)
Cd1-N2	2.318(2)	Cd1-N7	2.349(2)
Cd1-N5	2.394(2)	Cd1-O5	2.3992(19)
Cd2-O5	2.2655(17)	Cd2-N8	2.298(2)
Cd2-N3	2.452(2)	Cd2-O2	2.424(2)
Cd2-O1	2.602(2)	Cd2-O4	2.5454(19)
Cd2-N1	2.314(2)		

Bond angles (°)

O7-Cd1-O4	113.67(7)	O7-Cd1-N2	95.04(7)
O4-Cd1-N2	89.94(7)	O7-Cd1-N7	87.11(7)
O4-Cd1-N7	87.15(7)	N2-Cd1-N7	176.90(8)
O7-Cd1-N5	104.85(7)	O4-Cd1-N5	141.18(7)
N2-Cd1-N5	91.38(7)	N7-Cd1-N5	90.23(7)
O7-Cd1-O5	170.84(6)	O4-Cd1-O5	72.30(6)
N2-Cd1-O5	91.85(7)	N7-Cd1-O5	86.26(7)
N5-Cd1-O5	68.89(7)	O5-Cd2-N8	91.45(7)
O5-Cd2-N1	89.68(7)	N8-Cd2-N1	174.22(8)
O5-Cd2-O2	105.16(7)	N8-Cd2-O2	93.97(8)
N1-Cd2-O2	80.26(8)	O5-Cd2-N3	134.49(7)
N8-Cd2-N3	95.09(7)	N1-Cd2-N3	88.15(7)
O2-Cd2-N3	119.16(7)	O5-Cd2-O4	69.95(6)
N8-Cd2-O4	96.50(7)	N1-Cd2-O4	89.22(7)
O2-Cd2-O4	168.52(7)	N3-Cd2-O4	64.57(6)
O5-Cd2-O1	154.93(7)	N8-Cd2-O1	81.03(7)
N1-Cd2-O1	95.60(7)	O2-Cd2-O1	52.13(7)
N3-Cd2-O1	70.31(7)	O4-Cd2-O1	134.42(6)

Table S2. Selected bond lengths (Å) and angles (°) for **2**.

Bond distances (Å)

Cu1-O4	1.963(4)	Cu1-O1	1.974(4)
Cu1-N4	1.992(5)	Cu1-N3	1.992(5)
Cu1-N1	2.327(6)		

Bond angles (°)

O4-Cu1-O1	167.7(2)	O4-Cu1-N4	90.91(19)
O1-Cu1-N4	88.2(2)	O4-Cu1-N3	90.39(19)
O1-Cu1-N3	90.1(2)	N4-Cu1-N3	177.6(3)
O4-Cu1-N1	113.3(2)	O1-Cu1-N1	79.01(19)
N4-Cu1-N1	94.1(2)	N3-Cu1-N1	87.2(2)

(a)

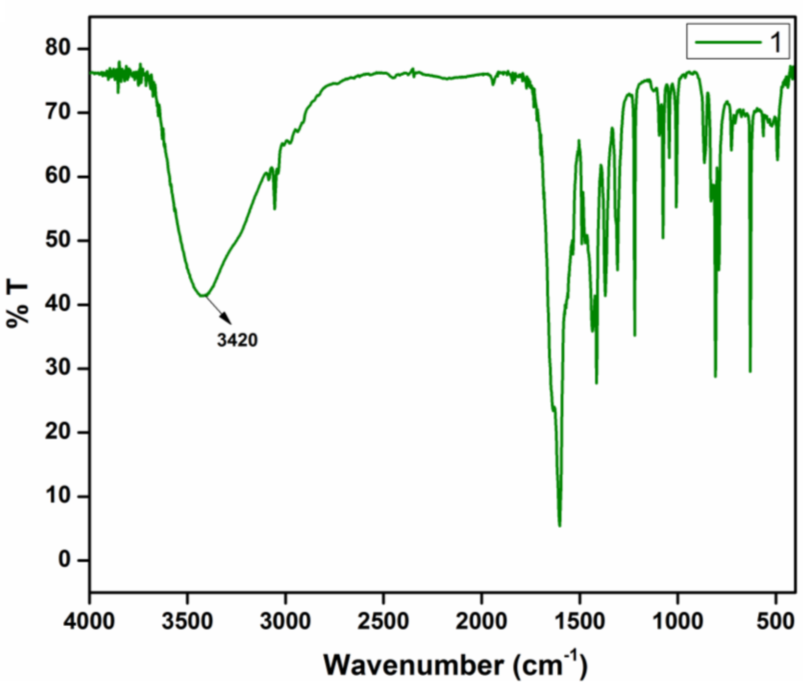

(b)

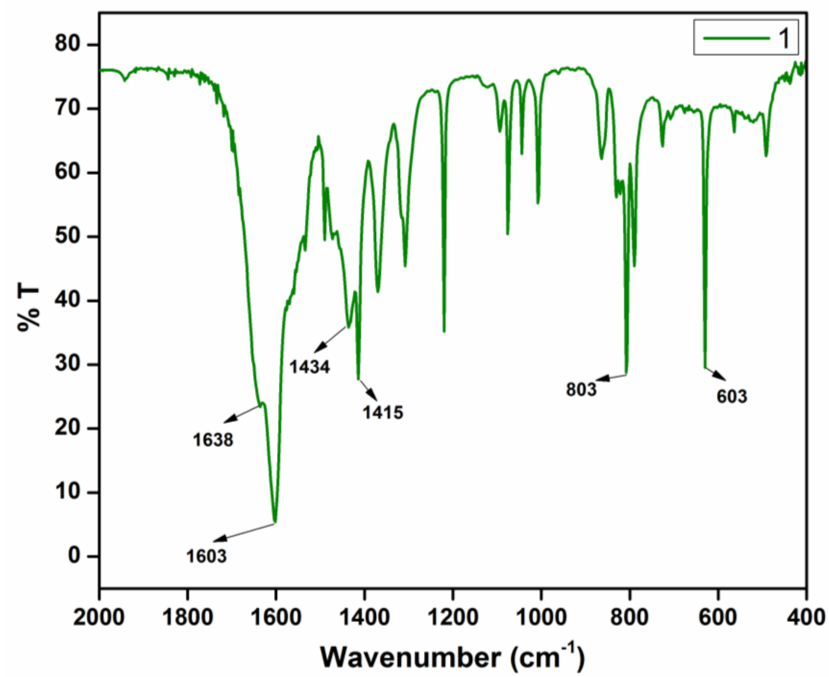

Fig. S3 (a) Full and (b) expanded region of the FTIR spectrum of **1**.

(a)

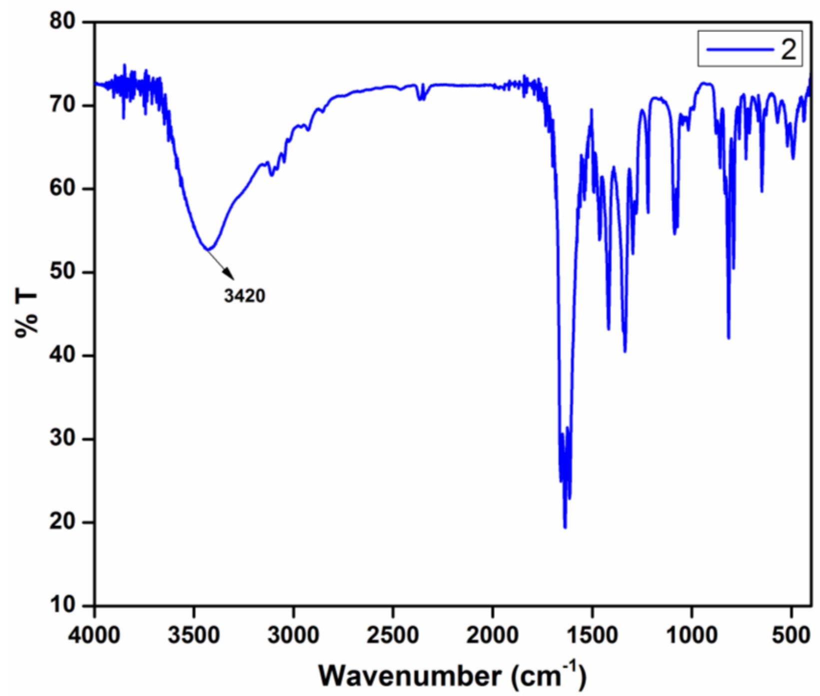

(b)

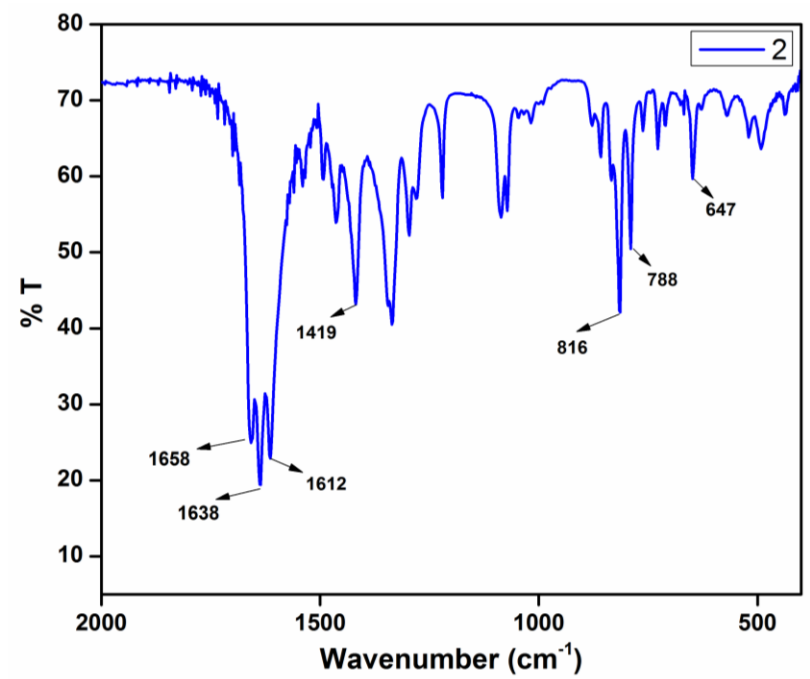

Fig. S4 (a) Full and (b) expanded region of the FTIR spectrum of **2**.

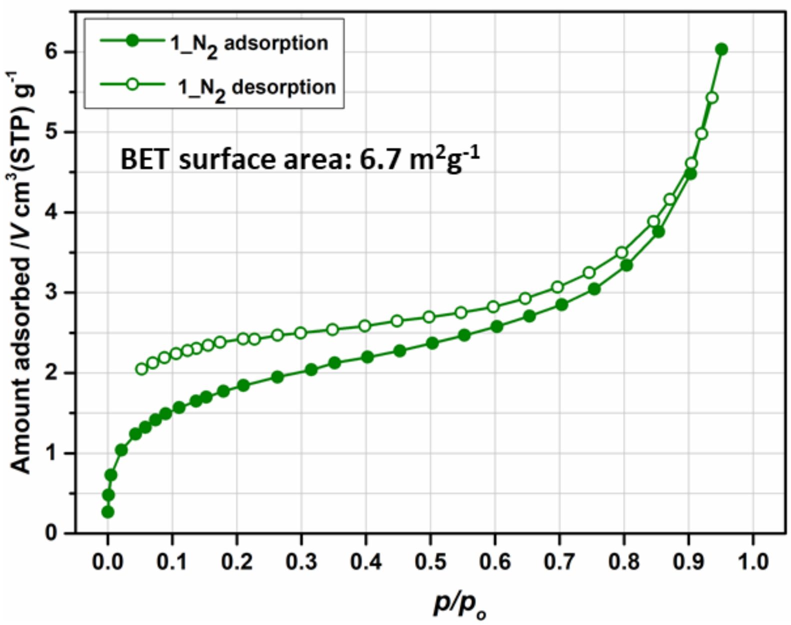

Fig. S5 N_2 adsorption isotherm of **1** at 77 K.

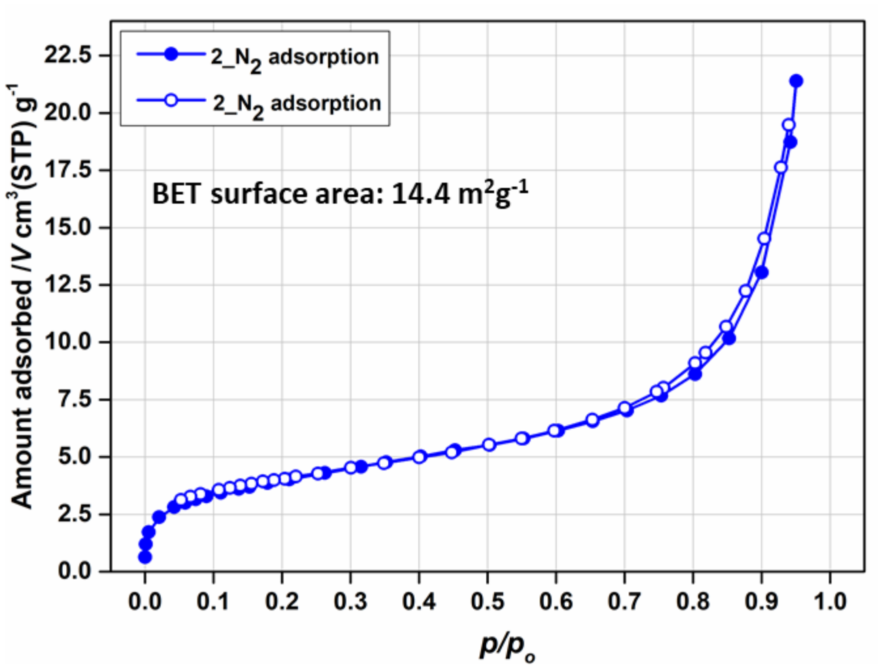

Fig. S6 N_2 adsorption isotherm of **2** at 77 K.

Calculation of isosteric heat of adsorption

A virial-type expression consisting of the temperature dependent virial parameters ai and bi were employed to calculate the isosteric heat of absorption for CO_2 at 263 K, 273 K and 298 K. The virial type expression is given below:

$$\ln(P) = \ln(N) + \frac{1}{T}\sum_{i=0}^{m} a_i\, N^i + \sum_{j=0}^{n} a_j\, N^j$$

where, P is the pressure expressed in Torr, N is the amount adsorbed in mmol/g, T is the temperature in K, a_i and b_i is the virial coefficients, and m, n represent the number of coefficients required to adequately describe the isotherms (m and n were gradually increased until the contribution of *a* and *b* coefficients added further were negligible towards the overall final fit, and the average value of the squared deviations from the experimental values was minimized). The values of the virial coefficient a_0 to a_i were taken to calculate the isosteric heat of adsorption using the following expression.

$$Q_{st} = -R\sum_{i=0}^{m} a_i\, N^i$$

Q_{st} is the coverage dependent isosteric heat of adsorption and R is the universal gas constant. At zero loading, the isosteric heat of adsorption (Q_{st}) for **1** and **2** are found to be 29.1 $kJmol^{-1}$ and 23.4 $kJmol^{-1}$, respectively.

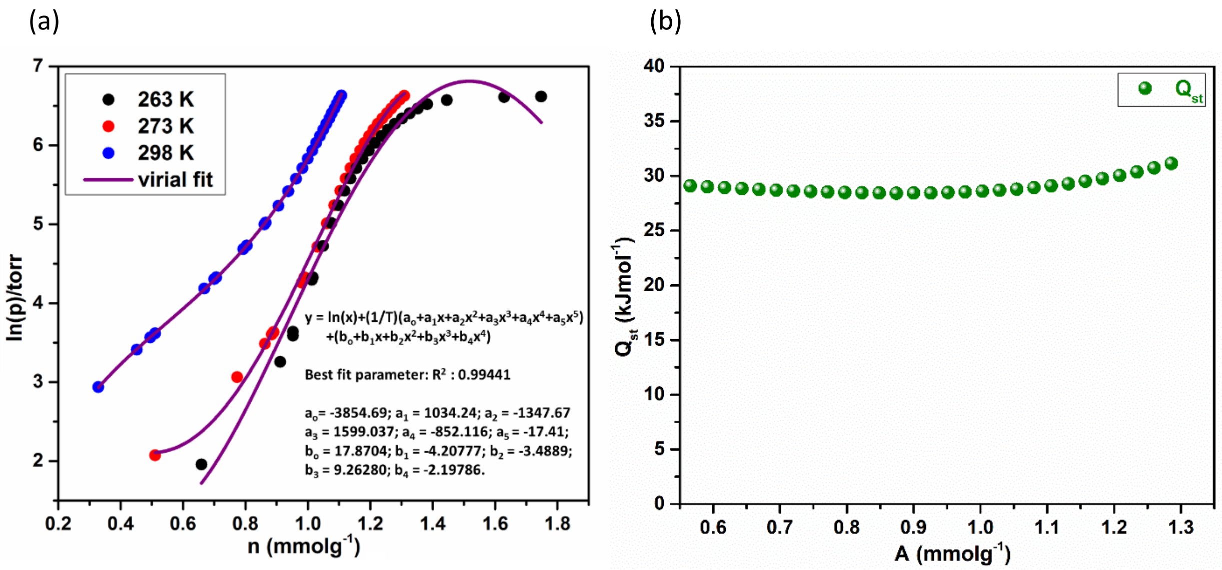

Fig. S7 Fitting (violet solid lines) of the CO_2 adsorption isotherms for **1** measured at 263 K (black circle), 273 K (red circle), and 298 K (blue circle) using the virial method to estimate the Q_{st} value.

(a)

(b)

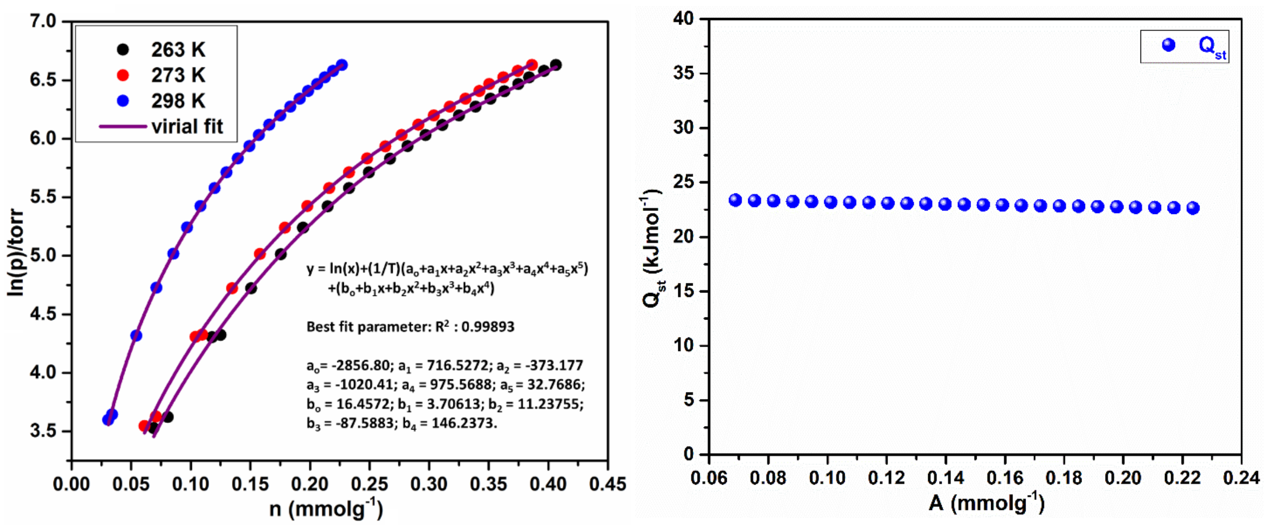

Fig. S8 Fitting (violet solid lines) of the CO_2 adsorption isotherms for **2** measured at 263 K (black circle), 273 K (red circle), and 298 K (blue circle) using the virial method to estimate the Q_{st} value.

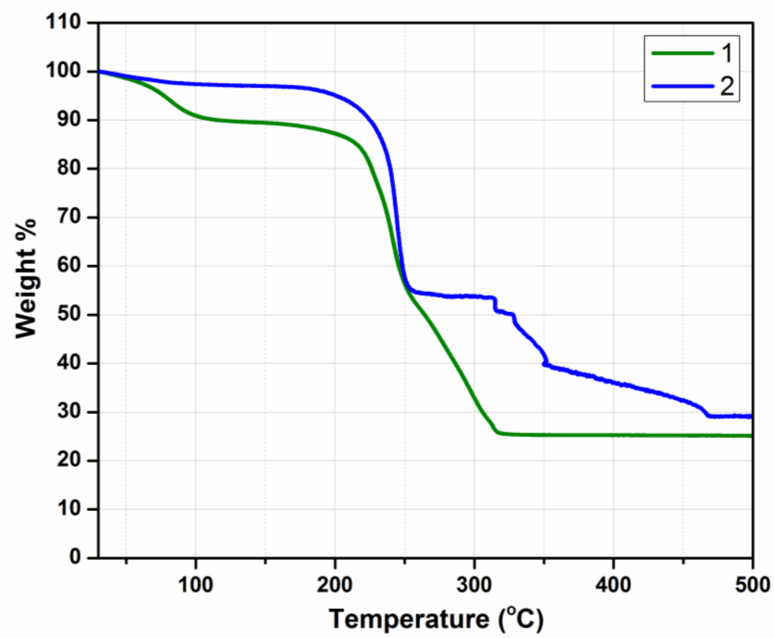

Fig. S9 TGA profiles of **1** and **2**.

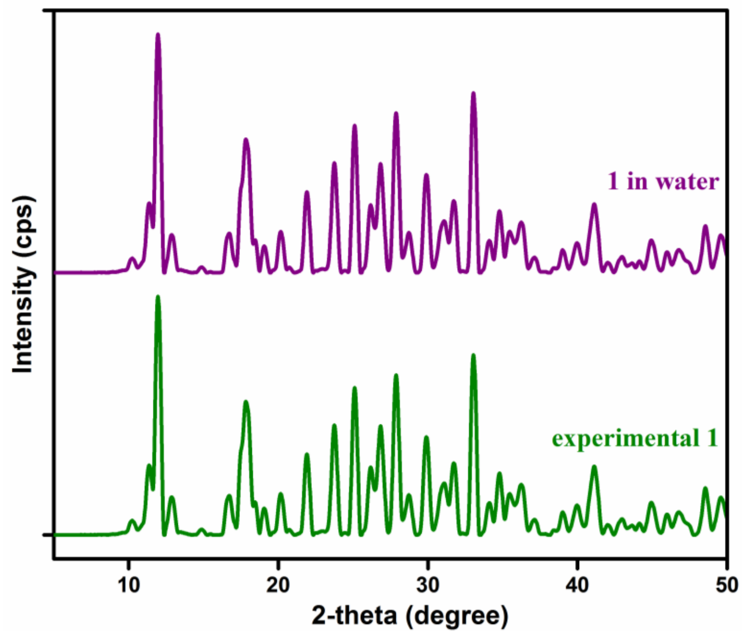

Fig. S10 PXRD patterns of as-synthesized **1** and after immersing it in water.

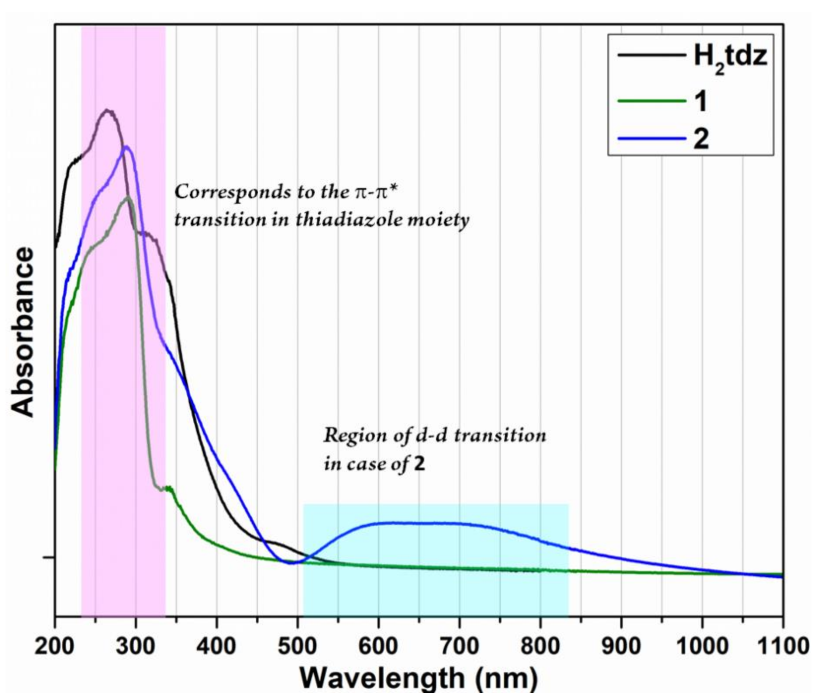

Fig. S11 Solid-state reflectance spectra of **1** and **2**.

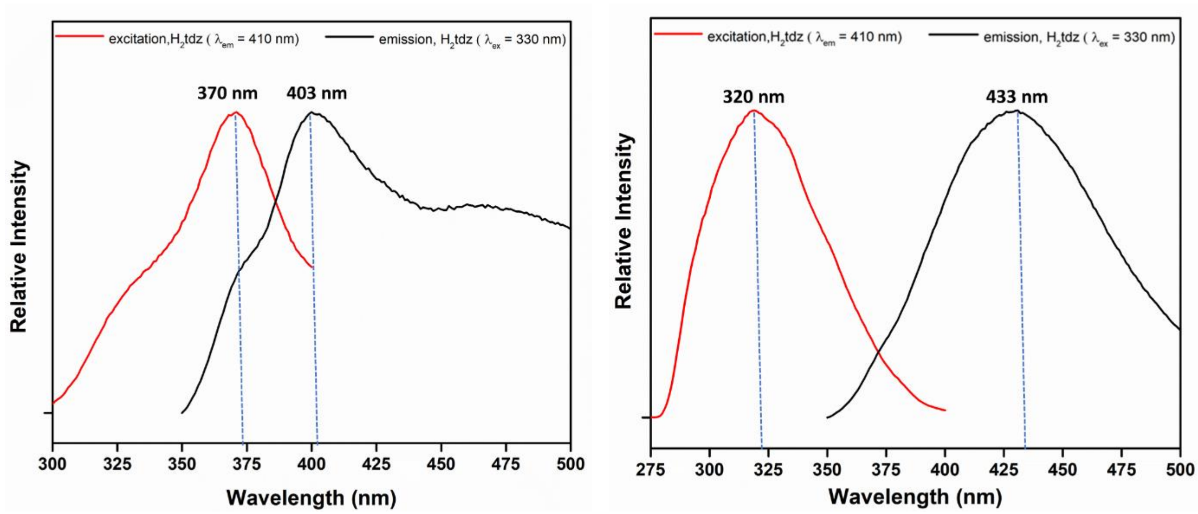

Fig. S12 Excitation and emission spectra of H_2tdz in solid-state (left) and in water (right).

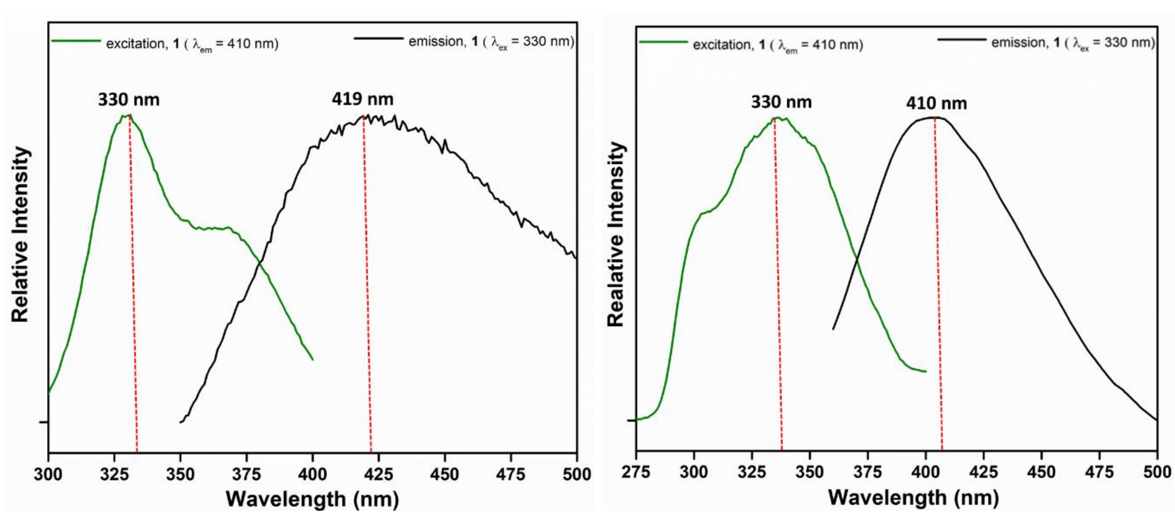

Fig. S13 Excitation and emission spectra of **1** in solid-state (left) and dispersed in water (right).

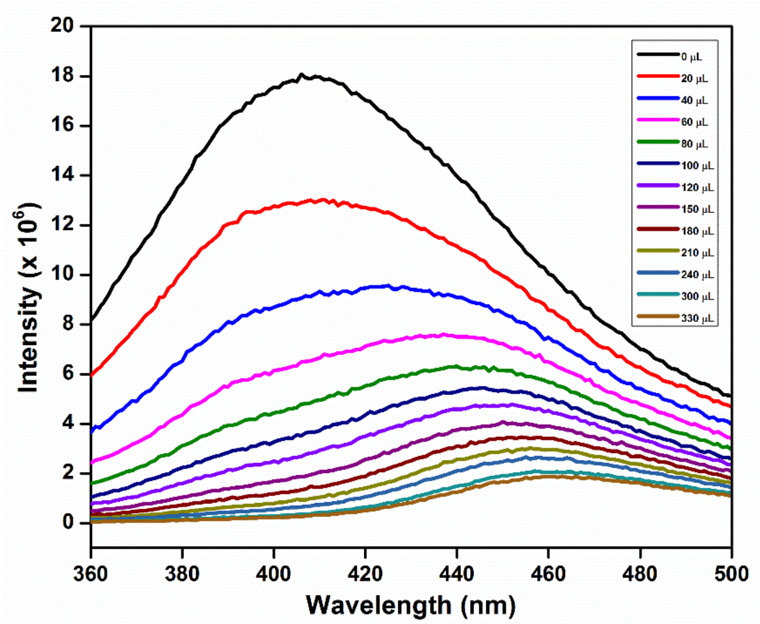

Fig. S14 Change in emission spectra of **1** dispersed in water upon incremental addition of 2,4-DNP solution (2 mM) in water.

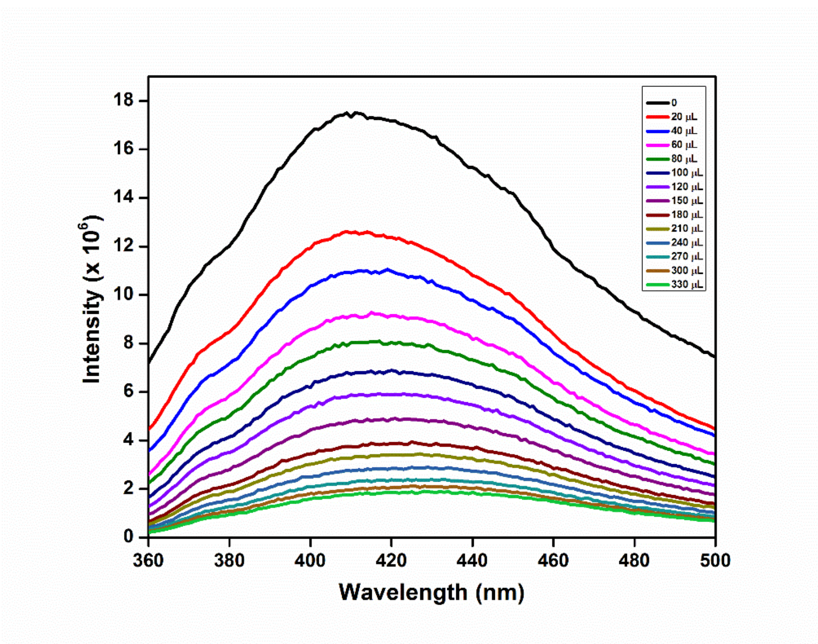

Fig. S15 Change in emission spectra of **1** dispersed in water upon incremental addition of 4-NP solution (2 mM) in water.

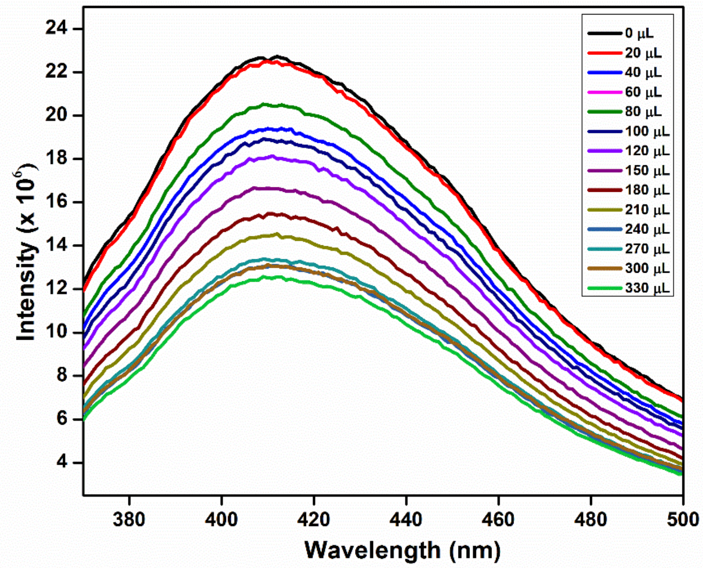

Fig. S16 Change in emission spectra of **1** dispersed in water upon incremental addition of TNT solution (2 mM) in water.

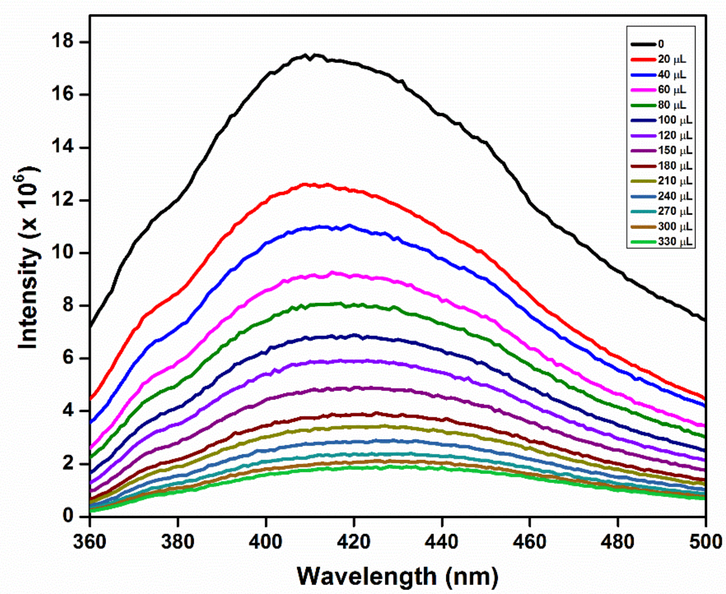

Fig. S17 Change in emission spectra of **1** dispersed in water upon incremental addition of 2,6-DNT solution (2 mM) in water.

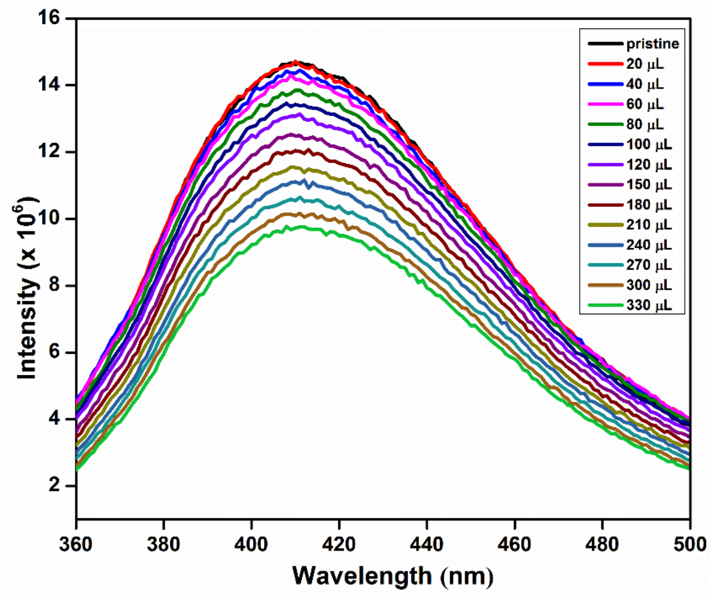

Fig. S18 Change in emission spectra of **1** dispersed in water upon incremental addition of 2,4-DNT solution (2 mM) in water.

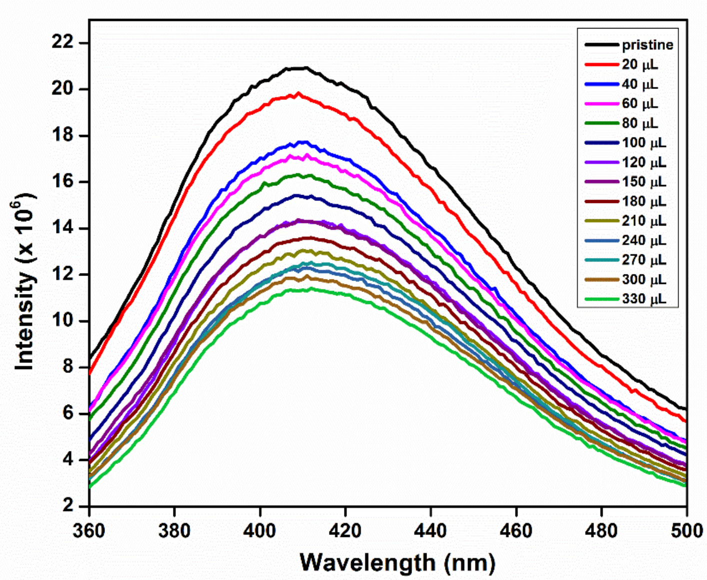

Fig. S19 Change in emission spectra of **1** dispersed in water upon incremental addition of 1,3-DNB solution (2 mM) in water.

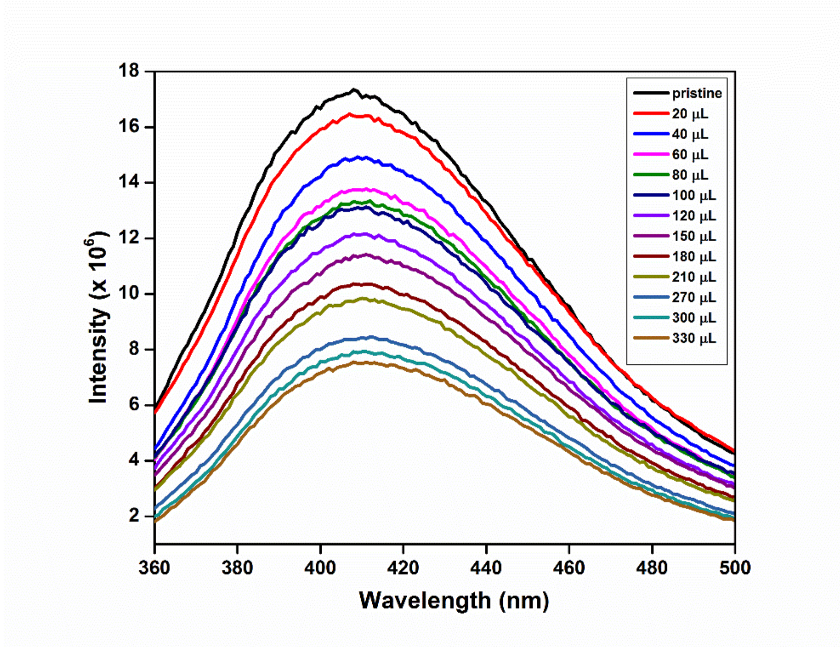

Fig. S20 Change in emission spectra of **1** dispersed in water upon incremental addition of NB solution (2 mM) in water.

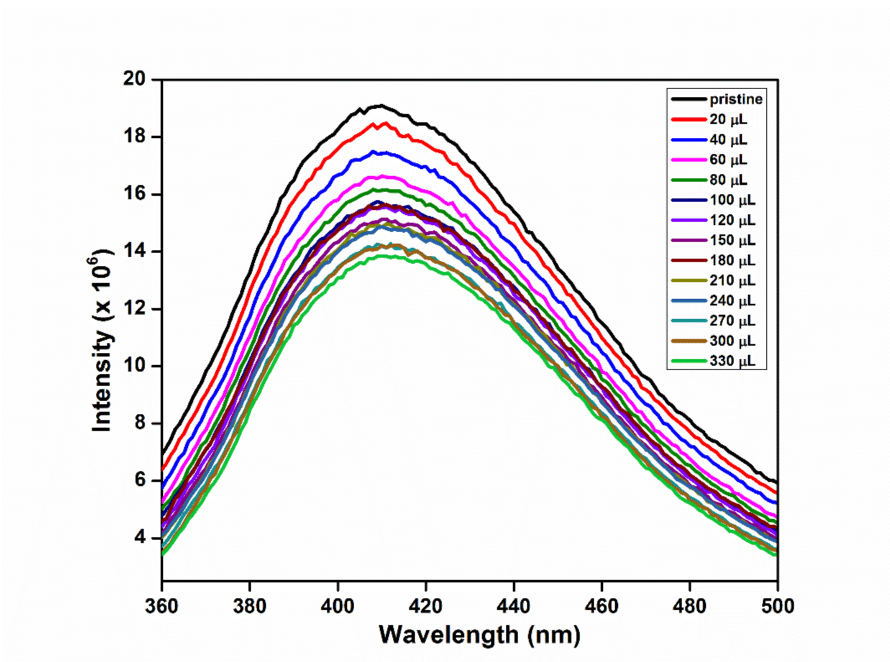

Fig. S21 Change in emission spectra of **1** dispersed in water upon incremental addition of NM solution (2 mM) in water.

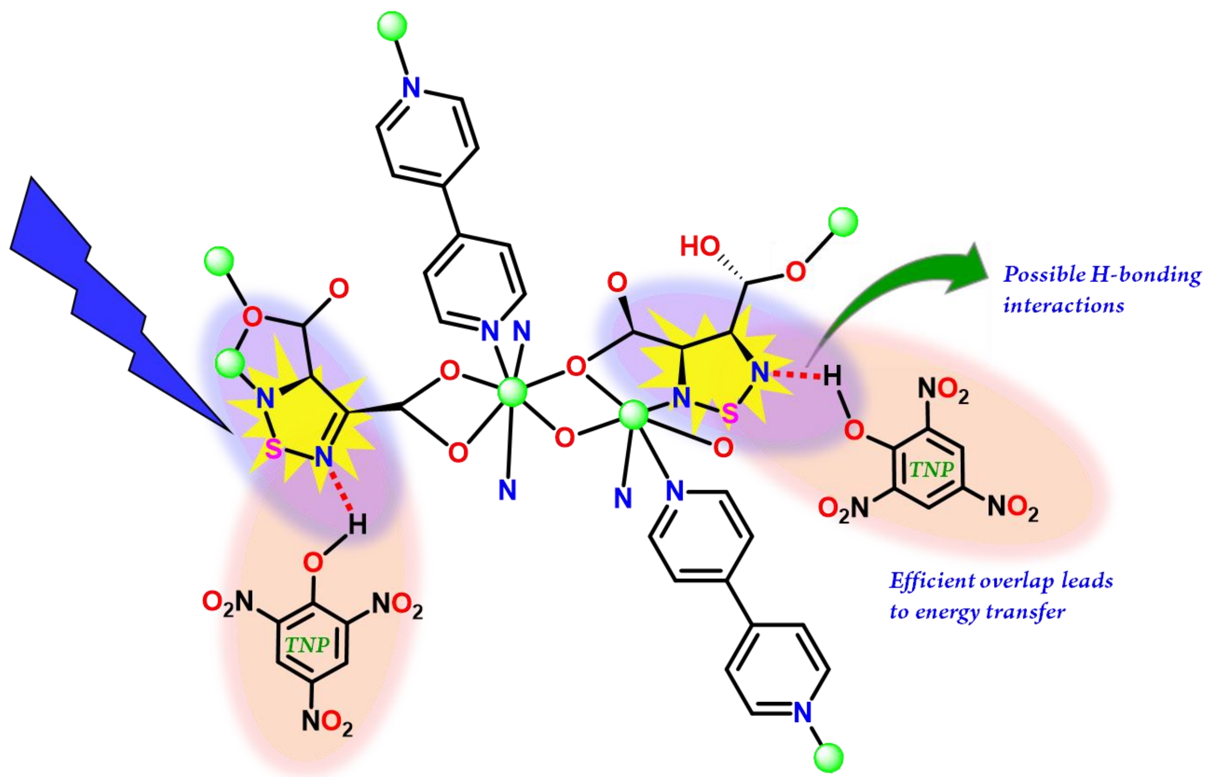

Scheme S1 Possible H-bonding interactions between the thiadiazole moiety in **1** and TNP molecules.

(a)

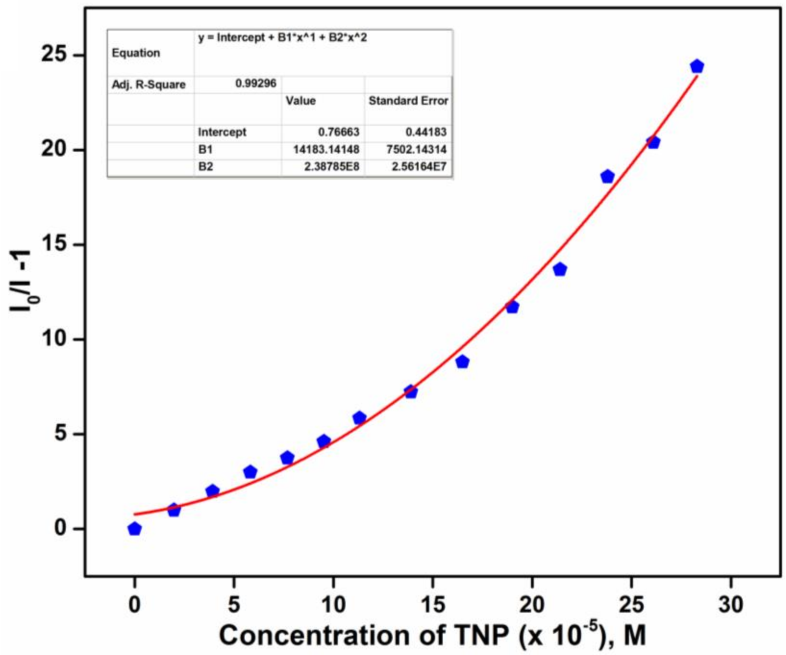

(b)

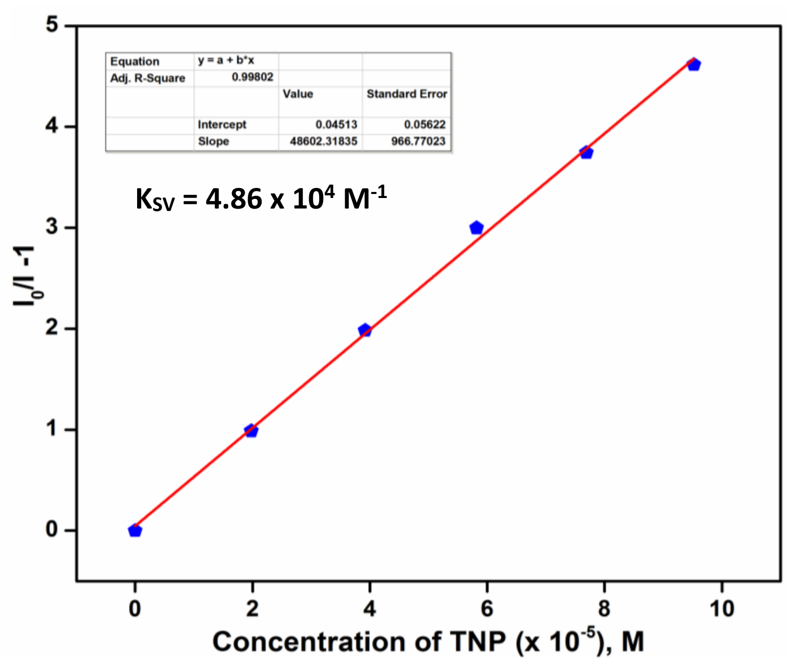

Fig. S22 Stern-Volmer (SV) plot of **1** for TNP. The relative fluorescence intensity is linear with TNP concentration in the lower region, $I_0/I = 1 + 48602.32[TNP]$ ($R^2 = 0.998$).

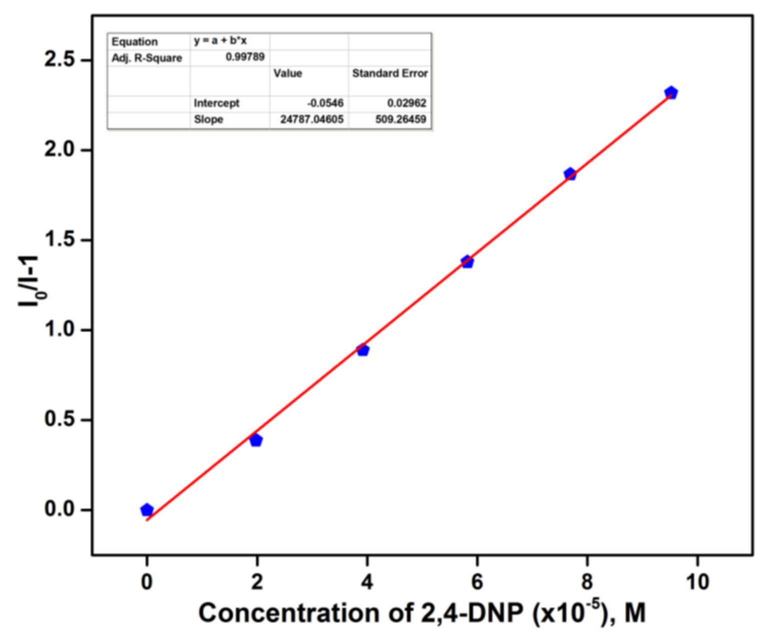

Fig. S23 Stern-Volmer (SV) plot of **1** for 2,4-DNP. The relative fluorescence intensity is linear with TNP concentration in the lower region, $I_0/I = 1 + 24787.05[2,4\text{-DNP}]$ ($R^2 = 0.998$).

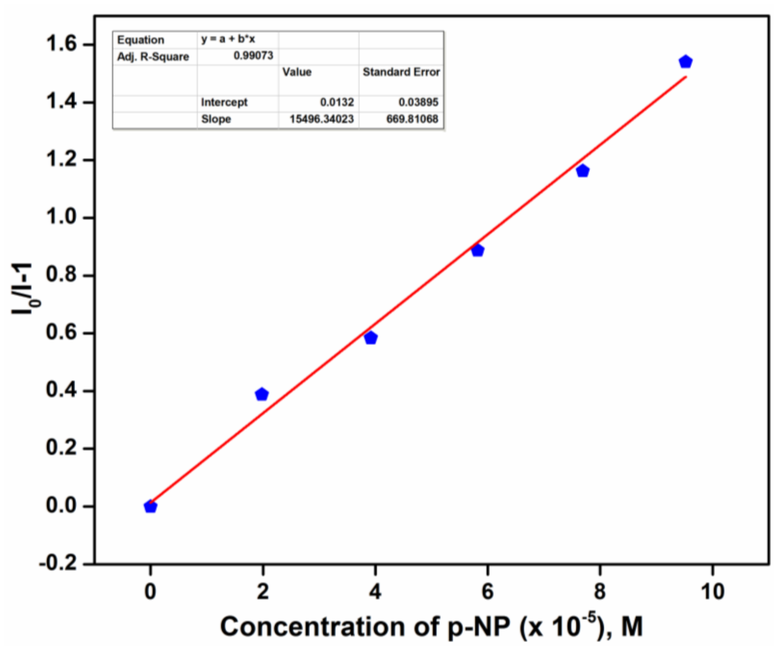

Fig. S24 Stern-Volmer (SV) plot of **1** for 4-NP. The relative fluorescence intensity is linear with TNP concentration in the lower region, $I_0/I = 1 + 15496.34[4\text{-NP}]$ ($R^2 = 0.991$).

Table S3. Comparison of literature reports for MOFs as sensors of NAEs.

MOF	K_{SV} (M^{-1})	Detection Limit	Medium	Reference
$\{[Cd_2(tdz)_2(4,4'\text{-bpy})_2]\cdot 6.5H_2O\}_n$ (1)	4.86 x 10^4	6.3 x 10^{-6} M (1.4 ppm)	H_2O	**This work**
$[Zr_6O_4(OH)_4(BTDB)_6]\cdot 8H_2O\cdot 6DMF$	2.49 x 10^4	1.63 x 10^{-6} M	MeOH	*CrystEngComm*, 2016, **18**, 3104–3113.
$\{[Cd(BIDPT)(oba)]\cdot 0.5H_2O\}n$ (1) and $\{[Zn(BIDPT)(4,4'\text{-sdb})]\cdot 2.25H_2O\}_n$ (2)	2.33 x 10^4 and 2.78 x 10^4	NA NA	DMF	*Inorg. Chem. Commun.*, 2016, **66**, 51-54.
$[Zn_4(DMF)(Ur)_2(2,6\text{-NDC})_4]_n$	10.83 x 10^4	NA 1.63 ppm	H_2O	*Cryst. Growth Des.*, 2015, **15**, 4627−4634
$Zr_6O_4(OH)_4(L)_6$	2.9 x 10^4	2.6 x 10^{-6} M	H_2O	*Chem. Commun.*, 2014, **50**, 8915-8918.
$[Cd_3(TPT)_2(DMF)_2]\cdot 0.5H_2O]_n$	6.56 x 10^4	NA	EtOH	*Dalton Trans.*, 2015, **44**, 230-236.
$[Zn_2(NDC)_2(bpy)]\cdot Gx$	0.4 x 10^4	NA	EtOH	*J. Mater. Chem. C*, 2014, **2**, 10073-10081.
$\{Zn_2(tpbn)(2,6\text{-NDC})_2\}_n$ (1) and $\{[Zn_2(tphn)(2,6\text{-NDC})_2]\cdot 4H_2O\}_n$ (2)	5.907 x 10^3 and 2.464 x 10^3	11 ppm and 19 ppm	H_2O	*Inorg. Chem.*, 2017, **56**, 14556–14566.
$[Zn_2(L)_2(dpyb)]_n$ (MOF-1) and $[Zn(L)(dipb)](H_2O)_2$ (MOF-2)	2.40 x 10^4 and 2.46 x 10^4	NA	DMA	*Chem. Commun.*, 2015, **51**, 8300-8303.
$[Zr_6O_4(OH)_6(L)_6]_n$	5.8 x 10^4	0.4 ppm	H_2O	*Dalton Trans.*, 2015, **44**, 15175-15180.
$[Tb(1,3,5\text{-BTC})]_n$	3.4 x 10^4	8.1 x 10^{-8} M	EtOH	*J. Mater. Chem. A*, 2013, **1**, 8745-8752.
$[La(TPT)(DMSO)_2]\cdot H_2O$	9.89 x 10^4	NA	EtOH	*Dalton Trans.*, 2015, **44**, 13340-13346.

NA: Not applicable/not mentioned in the reports.

Calculation of detection limit

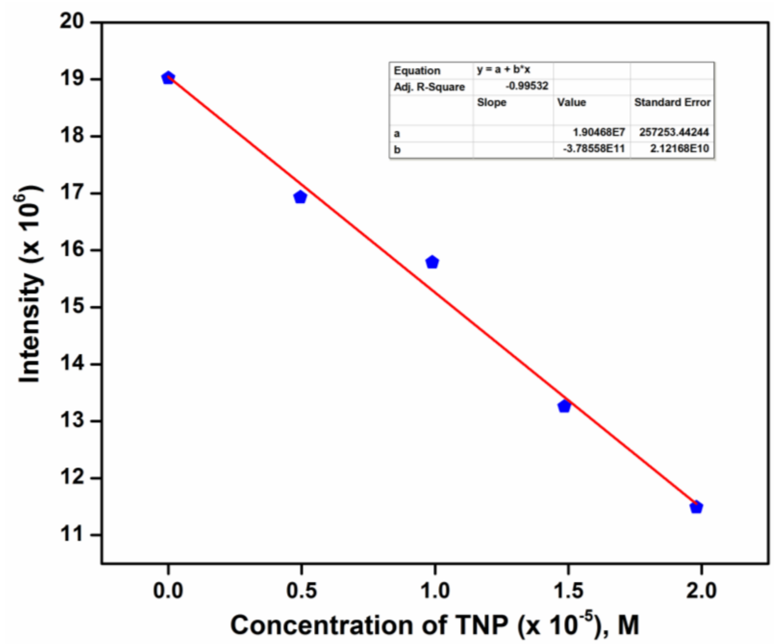

Fig. S25 Linear region of fluorescence intensity of probe upon addition of TNP to **1** at λ_{em} = 410 nm (λ_{ex} = 310 nm) (R^2 = 0.995).

Table S4. Calculation of standard deviation and detection limit.

Blank Readings (**1**)	Emission Intensity
Reading 1	1.81×10^7
Reading 2	1.72×10^7
Reading 3	1.75×10^7
Reading 4	1.90×10^7
Standard Deviation (σ)	0.0798×10^7

Slope from Graph (m)	3.7856×10^{11} M^{-1}
Detection Limit ($3\sigma/m$)	6.3 μM (**1.4 ppm**)

Detection limit was calculated using the following equation:
Detection limit = $3\sigma/m$
Where 'σ' is the calculated standard deviation from four blank measurements and 'm' is the slope obtained from the plot of fluorescence emission with increasing concentration of TNP.

Table S5. Average lifetime (τ) calculated for **1** before and after TNP addition.

	1	**1 + 20 μL TNP**	**1 + 60 μL TNP**
χ^2 **value**	1.27	1.10	1.18
τ1 (ns)	0.187	0.169	0.572
α1	0.368	0.376	0.150
τ2 (ns)	0.714	0.736	0.269
α2	0.246	0.259	0.208
τ3 (ns)	0.098	0.096	0.159
α3	0.865	0.814	0.464
Average τ (ns)	0.43	0.41	0.27

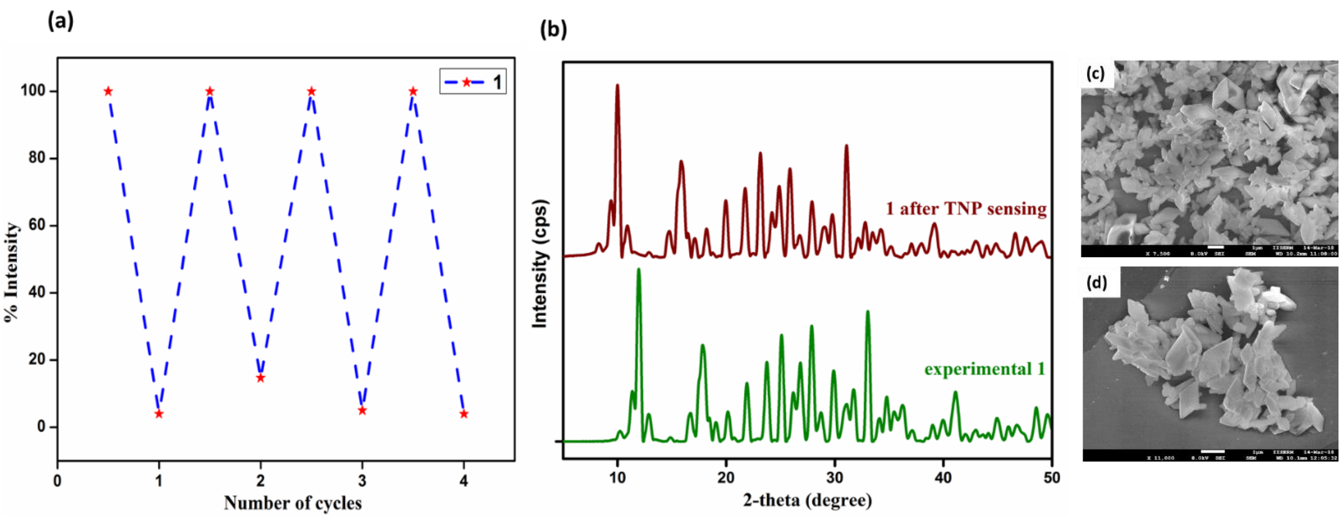

Fig. S26 Recyclability and stability of **1**. (a) The upper dots represent the initial fluorescence intensities, and the lower dots represent the intensities upon addition of 330 μL of the aqueous solution of TNP; (b) PXRD patterns of **1** before and after immersing in aqueous TNP solution, and FESEM images (c, d) of 1 before and after immersing in 2 mM aqueous TNP solution, respectively.

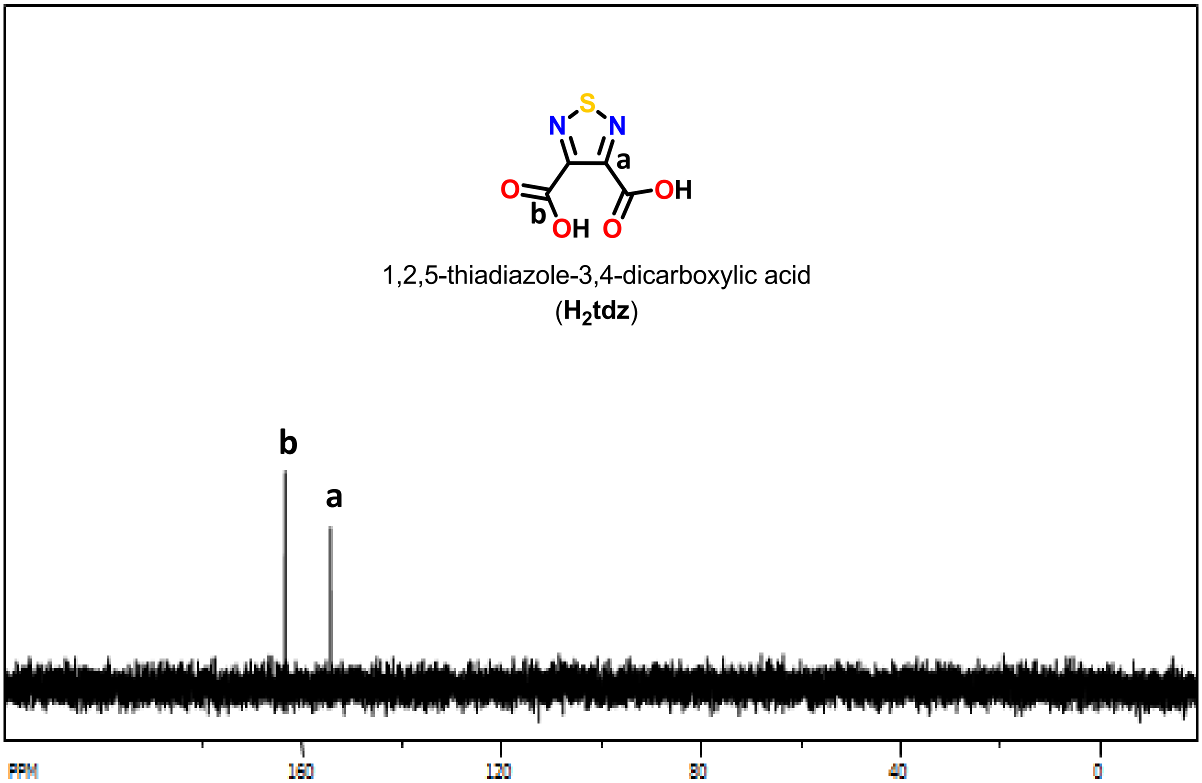

Fig. S27 ^{13}C NMR spectrum of H_2tdz in D_2O.

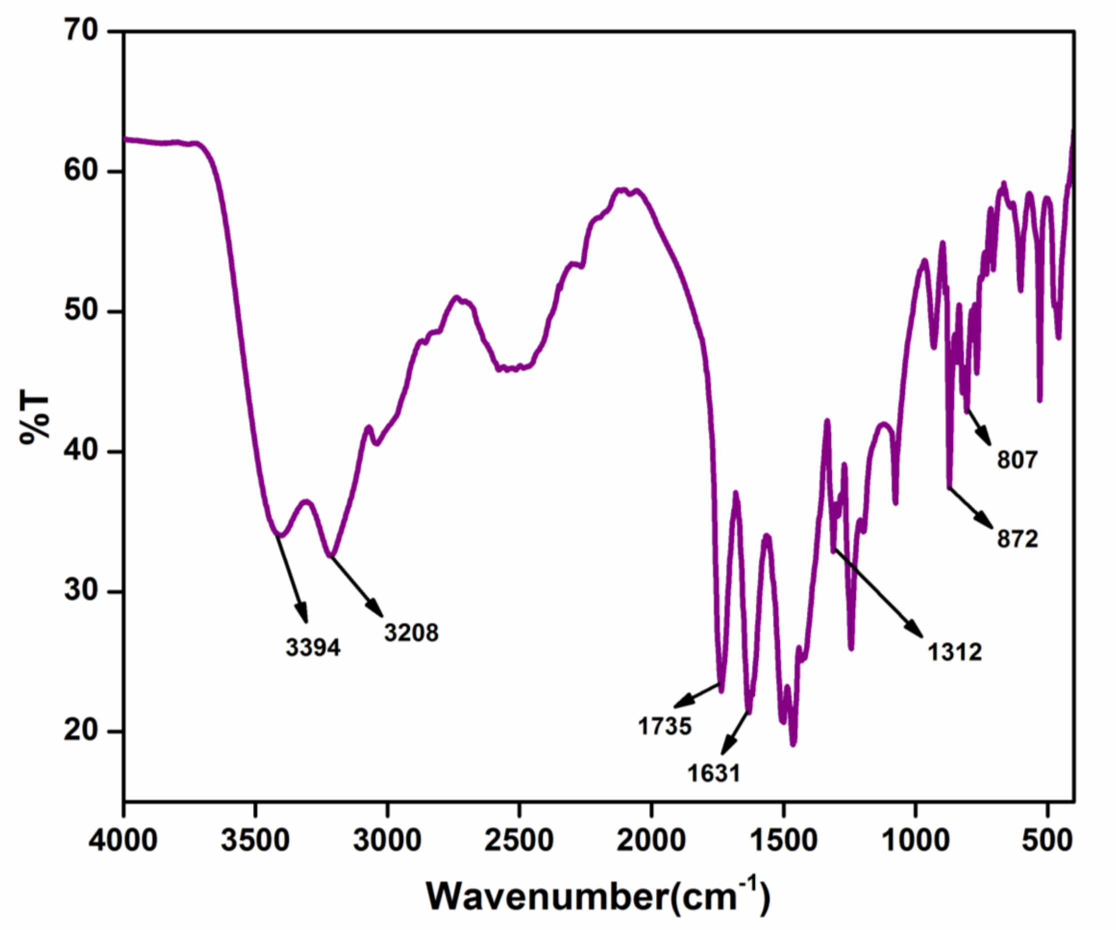

Fig. S28 FTIR spectrum of H_2tdz.

Selected FTIR Peaks (KBr, cm^{-1}): 1735 (C=O stretch), 1631 (C=N stretch), 1312 (C-C stretch), 872 (N-S stretch), 807 (C-S stretch).